Int. J. Electrochem. Sci., 16 **(2021)** Article ID: 210457, doi: 10.20964/2021.04.10

International Journal of
ELECTROCHEMICAL
SCIENCE
www.electrochemsci.org

Corrosion Behavior of 316 Stainless Steel Exposed to a Simulated Salt lake Atmospheric Environment under UV Illumination

Mingxiao Guo[1,2], *Xiao Lu*[1,2], *Junrong Tang*[1,2], *Chen Pan*[2,*], *Zhenyao Wang*[2,*]

[1] School of Materials Science and Engineering, University of Science and Technology of China, Shenyang 110016, China
[2] Institute of Metal Research, Chinese Academy of Sciences, Shenyang 110016, China
[*]E-mail: cpan@imr.ac.cn, zhywang@imr.ac.cn

Received: 16 October 2020 / *Accepted:* 28 December 2020 / *Published:* 28 February 2021

In this study, the corrosion mechanism of 316 stainless steel subjected to wet–dry cyclic accelerated corrosion test in a simulated salt lake atmosphere under ultraviolet (UV) illumination was investigated. The corrosion mechanism was investigated by analyzing the corrosion morphologies, corrosion products, in-situ electrochemical impedance spectroscopy (EIS) with micro-distance electrodes and Mott-Schottky measurements. The results revealed that UV illumination inhibited the corrosion rate of the 316 stainless steel with an increase in the corrosion time. In addition, UV illumination had no significant effect on the type of corrosion products but changed the relative amount of the corrosion products. Furthermore, the corrosion process of the 316 stainless steel under UV illumination was affected by the photovoltaic effect of the semiconductor corrosion products.

Keywords: Stainless steel; Atmosphere corrosion; In-situ EIS; Photovoltaic effect; Semiconductor

1. INTRODUCTION

Atmospheric corrosion is an electrochemical process that occurs in metals and its surrounding environment. Owing to the importance of atmospheric corrosion, tremendous attention have been devoted to investigate the effect of environmental factors such as temperatue [1, 2], relative humidity [3, 4], time of wetness [5], and salt particles in the air [6, 7], on the atmospheric corrosion of metals. In recent years, an increasing number of researchers have investigated the effects of ultraviolet (UV) illumination on the atmospheric corrosion of metals. Previous studies have reported that UV illumination has a significant effect on the atmospheric corrosion process of metals. For example, Song demonstrated that UV illumination significantly affected the corrosion behavior of weathering steels in NaCl atmosphere [8]. In addition, Liu revealed that the thickness of the rust layer of carbon steel increases, a

large number of voids and cracks are formed, and the corrosion rate is significantly accelerated under UV exposure [9]. Furthermore, Chen and Liang investigated the effect of UV illumination on the atmospheric corrosion of silver, and found that UV illumination promoted the decomposition of oxygen, accelerated the generation of silver oxide, and significantly accelerated the corrosion rate of silver [10, 11]. These studies attributed the promotion of the corrosion of metal by UV illumination to the photovoltaic effect of the semiconducting corrosion products.

Generally, stainless steels exhibit higher corrosion resistance than several metals under atmospheric conditions. The corrosion of stainless steel is performed as non-uinform corrosion, chloride-induced pitting corrosion. Tremendous efforts have been devoted to investigate the effect of UV illumination on the corrosion process of stainless steels in bulk solution. For example, Fujimoto revealed that UV illumination inhibited the pitting corrosion of stainless steel [12]. In addition, Macdonaled revealed that the pitting resistance of stainless steel was enhanced at low power densities but reduced at high power densities [13]. However, the corrosion behavior of stainless steels in atmospheric environment is relatively different from that in solution. Studies on the influence of UV illumination on the corrosion behavior of stainless steels in atmospheric environment are rare. There are hundreds of salt lakes in Northwest China, and the high rates of natural and high sea-salt deposition in these lakes aggravate the atmospheric corrosion in this region. The environmental parameters in a salt lake atmosphere are listed in Table 1. Moreover, the salt lake atmosphere remains more UV illumination than marine atmosphere. Previous studies have reported that the corrosion of stainless steel in a salt lake atmosphere is significantly different from that in a marine armosphere [14]. Therefore, it is important to extensively investigatet the effect of UV illumination on the corrosion behavior of stainless steel in salt lake atmosphere.

Table 1. Environmental conditions of the salt lake atmosphere

Average temperature (℃ $year^{-1}$)	Average rainfull (mm $year^{-1}$)	Average evaporation (mm $year^{-1}$)	Saline particles (mg m^{-2} day^{-1})	Natural deposition (g m^{-2} $mouth^{-1}$)	
				Soluble	Insoluble
17.5	38.3	3067	19.16	23.19	20.98

Because the corrosion process is an electrochemical process, the real-time detection technology of atmospheric corrosion based on electrochemical analysis has received significant attention in recent years. These technologies include atmospheric corrosion monitors (ACM) [15, 16] and Kelvin probes [17, 18]. However, some factors limit the further application of these methods: some are unsuitable for for practical field monitoring, while others only provide the severity of the degree of corrosion but cannot provide direct information on the prevailing electrochemical processes. In contrast, in-situ electrochemical impedance spectroscopy (EIS) technique is a non-destructive method for investigating the atmospheric corrosion of metals, and have been successfully applied to provide real-time and direct information on the corrosion behavior of metals [19-22].

In this study, the corrosion behavior of 316 stainless steel (316 SS) subjected to a simulated salt lake atmosphere, where relative humidity and temperature are controlled according to actual atmosphere, has been studied by in situ electrochemical impedance spectroscopy (EIS) with micro-distance electrodes and Mott-Schottky measurements, and the corrosion morphology and product composition of 316 stainless steel were also characterized. Furthermore, the influence of UV illumination on the corrosion mechanism was discussed. The combined results were used to elucidate the effect of UV illumination on the corrosion behavior of the 316 SS in a salt lake atmosphere.

2. EXPERIMENTAL

2.1 Sample preparation and electrode preparation

In this study, 316 SS with an elemental composition (in mass%) of 10.7% Ni, 16.8% Cr, 2.2% Mo, 1.28% Mn, 0.04% N, 0.3% Si, 0,04% C, 0.26P, 0.002%S and Fe balance, was used as the test material. Plate specimens with a dimension of 50 mm × 25 mm × 3 mm were cut from the test sample and used for the corrosion morphology and product composition analysis. In addition, plate specimens with a dimension of 10 mm × 10 mm × 3 mm were cut from the test sample, and used for the EIS analysis. To facilitate the collection of electrical signals, comb shaped micro-distance electrodes were prepared from the 316 SS plates according to previous studies [23]. The plates were separated by a thin insulation layer, after which they were embedded in epoxy. The distance between the two plates was limited to approximately 60 μm. Subesquently, the micro-distance electrodes were grounded with a 2000 # grade emery paper, after which they were stored in a desiccator at least 24 h, and then subjected to the wet – dry cyclic corrosion test.

2.2 Wet–dry cyclic accelerated test

To investigate the effects of UV illumination on the corrosion behavior of 316SS exposed to a simulated salt lake environment, the Weiss-Voetsch temperature and climatic test system was employed for the wet–dry cyclic corrosion test. The samples used for wet–dry cyclic corrosion test were divided into two layers in the the test chamber: the upper layer was exposed to UV illumination, and the lower layer was not exposed to UV illumination. The two layers were separated by a radiation-proof material. A 15 W quartz UV lamp, which generated UV illumination in the spectral range of 290-400 nm, was used as the light source. The UV intensity of the exposed sample surface was 2.4 W/m^2, as measured by a UVAB light meter (Tenmars-TM213) [24].

The wet–dry cyclic corrosion test was conduted for a total of 60 d, and included the following steps within 48 h: (1) coating the samples surface with 20 $\mu L/cm^2$ of 0.1 mol/L $MgCl_2$ (simulating a salt lake atmosphere) and oven drying at 40 ºC, (2) wetting the samples in a test box set at 30 ºC and 80% relative humidity for 60 min, with the UV light source turned off, (3) drying the samples in a box maintained at 30 ºC and 20% relative humidity for 120 min, with the UV light source turned on, and (4) repeating steps (2) and (3) 15 times.

2.3 Electrochemical measurements

Electrochemical tests, including the in-situ EIS and Mott-Schottky test were conducted to investigate the effect of illumination on the corrosion behavior of the 316 SS in a simulated salt lake atmosphere. Owing to the possible incertitude of the corrosion measurements, three parallel samples were used for all electrochemical measurements in each group. For the in-situ EIS experiments, the test frequency was set between 100 kHz to 10 mHz, and the scanning frequency during the test was always carried out from high to low frequency. The measured EIS data were fitted using a commercial software "Zsimpwin". In addition, the semiconductor properties of the passive film were evaluated by Mott-Schottky tests. A traditional three-electrode glass cell (i.e., the exposed sample, a platinum plate, and a saturated calomel electrode (SCE) were used as the working electrode, counter electrode and reference electrode, respectively) was used for Mott-Schottky measurements at room temperature. Prior to the Mott-Schottky tests, a 1800 s open-current potential (OCP) test was carried out and a stable OCP value was obtained. To avoid the interference of frequency with capacitance, a frequency of 1000 Hz was selected [25]. The Mott-Schottky diagram was measured in the potential (V_{SCE}) range from -0.6 - 0.3 V_{SCE}, at a potential step of 20 mV.

2.4 Characterization of corrosion products

The two-dimensional (2D) and three-dimensional (3D) surface morphologies of the corrosion samples were recorded using a stereomicroscope (Zeiss Stemi 508) and non-contact laser scanning confocal microscope (LSCM, Zeiss LSM-700). The surface roughness was also recorded using LSCM. The composition of the corrosion products was analyzed by X-ray photoelectron spectroscopy (XPS, ESCALAB250) with Al Kα excitation (hν=1,486.6 eV). The X-ray source and the analyzer pass energy were 50.0 eV. The current of the measured sample during the experiment was 2 mA, and the bombardment area was 2 mm × 2 mm. The binding energy was calibrated using standard carbon contamination (284.6 eV). The XPS data were processed using software of XPSPEAK 4.1 softare.

3. RESULTS AND DISCUSSTION

3.1. Electrochemical impedance spectroscopy measurements

EIS is an effective technique for investigaintg the corrosion behaviors of materials because it can provide non-destructive estimation of the corrosion rate and determine the mechanisms of the interface processes related to corrosion [23]. In this study, in-situ EIS analysis was carried out to directly investigate the corrosion process of 316 SS using specially micro-distance electrodes. Fig. 3a and b show the Nyquist diagrams of the 316 SS in simulated salt lake atmosphere with and without UV illumination at different corrosion times.

Fig. 3c shows the equivalent circuit constructed to fit the EIS results. In the equivalent circuit, R_s is the resistance of solution; Q_r and R_r are used to describe the dielectric properties of the corrosion

product layer; and Q_{dl} and R_{ct} represent the charge transfer process. Previous studies have reported that although the corrosion rate can be calculated from the polarization resistance (R_p), the correlation between the charge transfer resistance R_{ct} and the corrosion rate is more accurate than that of R_p because R_{ct} depends only on the faradaic processes of the charge transfer controlled corrosion. In addition, when the impedance response is more than the one time constant, the calculation of the corrosion rate using R_p results in an incorrect result [26,27]. In this study, the corrosion rate of the 316 SS exposed to the salt lake atmosphere was characterized using the reciprocal of the charge transfer resistance, R_{ct}. Fig. 3d shows the trend in the change of the reciprocal of R_{ct} with respect to the corrosion time. Obviously, the $1/R_{ct}$ value of the 316 SS under UV illumination was less than that without UV illumination, indicating that UV illumination inhibited the corrosion of 316 SS exposed to a simulated salt lake atmosphere. In previous studies, photoinhibition of nickel pitting corrosion was observed by S. Lenhart for the first time [28]. Next, P. Schmuki and H. Bohni reported that UV illumination resulted in a significant increase in pitting resistance of pure iron [29]. Subsequently, S. Fujimoto found that UV can promote a selective enrichment of Cr in passive film and suppress pitting corrosion on stainless steel [12]. In these reports, the inhibition of stainless steel pitting under UV illumination is consistent with the results obtained in salt lake atmosphere. However, the mechanism of UV illumination on the pitting corrosion of stainless steel has not been solved.

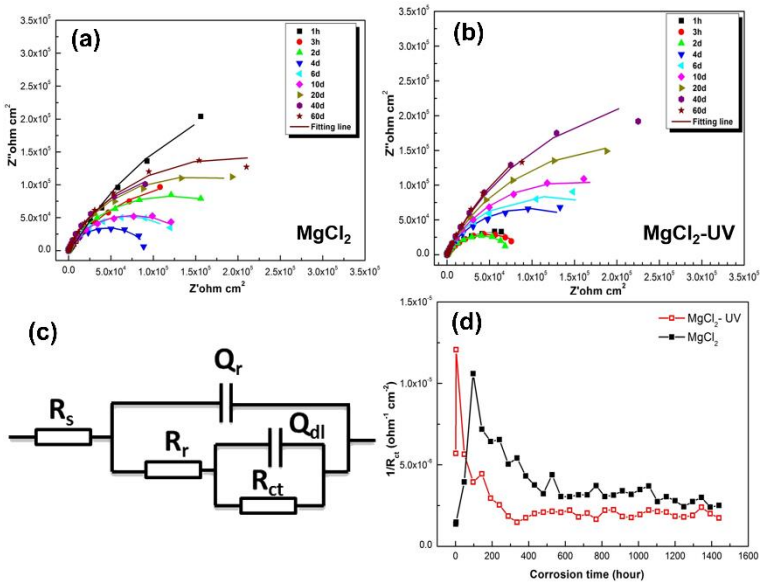

Figure 3. In-situ EIS results of 316 SS after different corrosion times: (a) Nyquist diagrams, without UV illumination, (b) Nyquist diagrams, with UV illumination, (c) Equivalent circuits and (d) Reciprocal of R_{ct}.

3.2. Mott-Schottky measurements

Fig. 4a. shows the Mott-Schottky plots of the 316 SS in simulated salt lake atmosphere with and without UV illumination after 10 and 60 d. Positive slopes were observed in the potential range from

−0.6–0.3 V_{SCE}, which could be attributed to the n-type semi-conductive passivation film. The Mott-Schottky equation for n-type semiconductors can be expressed as [30]:

$$C^{-2} = \frac{2}{\varepsilon\varepsilon_0 e N_D}\left(E - E_{FB} - \frac{kT}{e}\right) \quad (1)$$

where ε_0 is the dielectric constant of the free space (8.85× 10^{-14} F/cm), ε is the dielectric constant of the passive film, e is the electron charge (1.602 × 10^{-19} C), k is the Boltzman constant (1.38 × 10^{-23} J/K), and N_D is the carrier density of the passive film. E_{FB} and T are the flat band potential and the absolute temperature, respectively. kT/e is approximately 25 mV at room temperature, which is negligible. The carrier density value, N_D, of the 316 SS under UV illumination was calculated using the slope of the Mott-Schottky plots after linear fitting, and N_D is the expressed as follows:

$$K_{slope} = \frac{dC^{-2}}{dE} = \frac{2}{\varepsilon\varepsilon_0 e N_D} \quad (2)$$

$$N_D = \frac{2}{\varepsilon\varepsilon_0 e}\left(\frac{dC^{-2}}{dE}\right)^{-1} \quad (3)$$

Fig. 4b shows the N_D results of the 316 SS with and without UV illumination after 10 and 60 d. Several researchers [31-33] have reported that N_D reflects the conductivity of passive film: a lower N_D implies a higher film resistance, indicating the good protection of the passive film; A higher N_D value indicates that the passive film is more susceptive to pitting. In this study, the N_D value under UV illumination was low, indicating that the passive film exhibited good corrosion resistance. This indicates that UV illumination inhibited the corrosion rate of the 316 SS exposed to a simulated salt lake atmosphere.

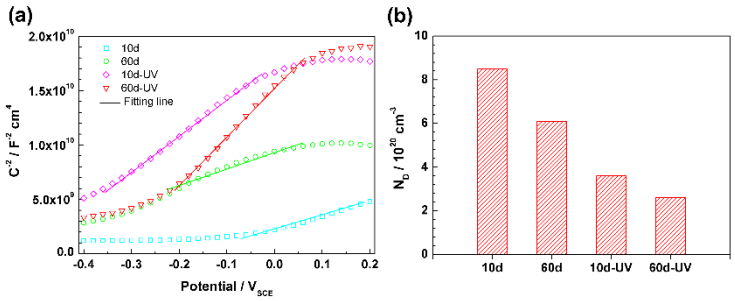

Figure 4. (a) Mott-Schottky plots of 316SS with UV illumination and without UV illumination after 10 and 60 days, (b) the values of carrier density N_D

3.3. Morphologies analysis of corrosion products

The surface macro-morphologies of the 316 SS with and without UV illumination after 10 d and 60 d were observed using a stereomicroscope. A few yellow rust layers were observed on the surface of the 316 SS exposed for 10 d without UV illumination (Fig. 5a). With an increase in the corroison time, the corrosion of the 316 SS aggravated and the yellow rust layer gradually covered the surface of the 316 SS (Fig. 5b). In contrast, under UV illumination, no rust layer was observed on the surface of the 316 SS after 10 d, and only a small amount of yellow rust layer appeared on the surface of the 316 SS after 60 d (Fig. 5c and d). In addition, naked white pits were formed on the surface of the 316 SS under

UV illumination or not. These pit morphologies were affected by the amount of $MgCl_2$, the changes of internal resistance between the anode and cathode area, and the ionic conductivity and diffusivity in highly concentrated solutions. These pit morphologies are consistent with our previous reports [34]. Macro-morphologies observation provides the most intuitive information on the degree of corrosion of the sample surface.

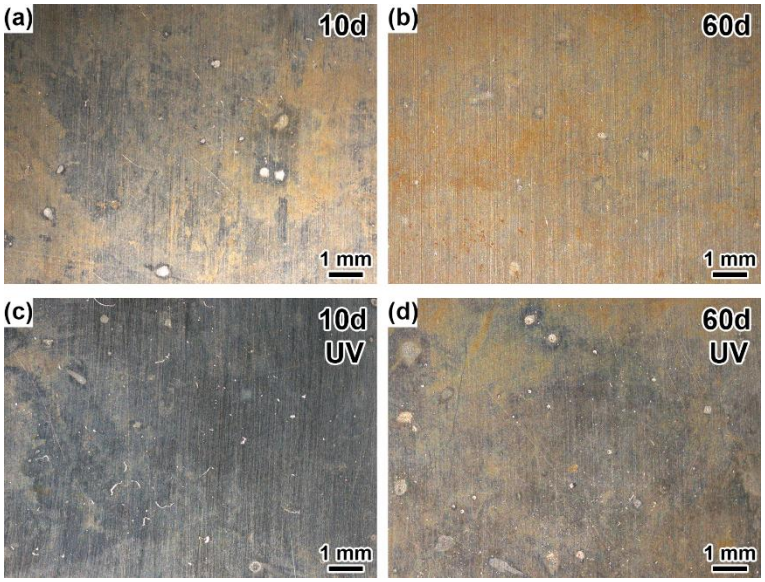

Figure 5. Stereomicroscope photos of the surface of 316 SS without (a and b) and with (c and d) UV illumination conditions: (a) and (c),10 days, (b) and (d) 60 days.

LSCM simultaneously provides information on the surface morphology and roughness information of the rust layer surface. Fig. 6 shows the 3D images and surface roughness values of the 316 SS with and without UV illumination. All the results were obtained for the same parameter and the area size The change in the image color can reflect the degree of corrosion of the sample surface. A green color indicates that the corrosion is close to the substrate of the stainless steels. With an increase in the corrosion products, the color gradually changed to green, yellow, orange and red sequentially. In addition, the surface roughness (Ra) measurements revealed that the Ra value of the 316 SS without UV illumination was approximately 0.359 μm after 10 d (Fig. 6a). After 60 d, the Ra value of the sample without UV illumination was approximately 0.754 μm (Fig. 6b). In contrast, the Ra values of the surface of the 316 SS under UV illumination after 10 and 60 d were 0.183 μm and 0.265 μm, respectively, which were signifitly lower than those without UV illumination (Fig. 6c and d). The aforedescribed results indicate that the corrosion of the 316 SS without UV illumination was severe compared to that with UV illumination. These results indicate that UV illumination significantly inhibited the corrosion of the 316 SS in a simulated salt lake atmosphere.

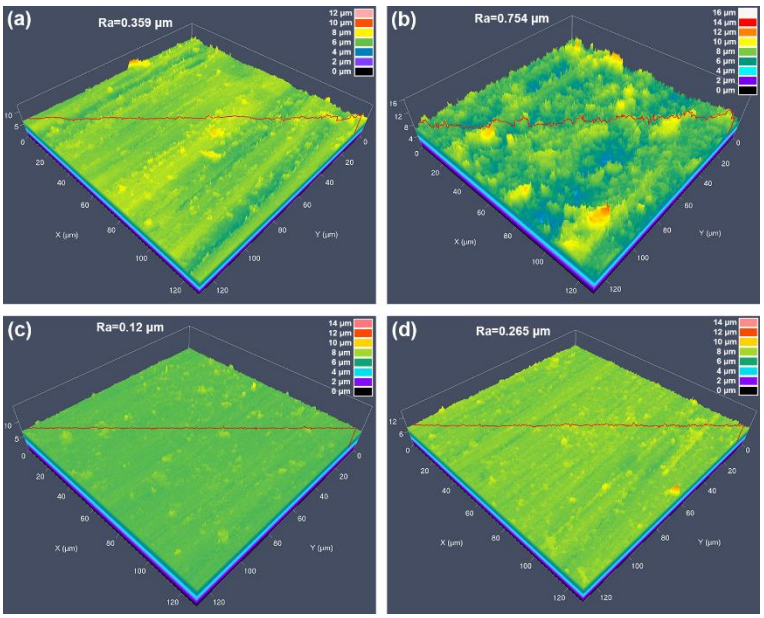

Figure 6. LSCM photos and 3D surface roughness values of the surface of 316 SS without (a and b) and with (c and d) UV illumination conditions: (a) and (c),10 days, (b) and (d) 60 days.

3.4. Composition of corrosion products

It is well known that the composition and evolution of corrosion products are closely related to the subsequent corrosion behavior of metals. Because only a small amount of corrosion products was deposited on the 316 SS surface, X-ray diffraction (XRD) analysis can not obtain the evolution information of the composition of the corrosion products as a function of corrosion time [35,36]. Thus, in this study, XPS was used to examine the composition of the corrosion products to understand the evolution of corrosion products as a function of the corrosion time. Fig. 7 shows the XPS spectra showing the composition of the corrosion products of the 316 SS with and without UV illumination after 10 and 60 d, particularly for the Fe $2p_{2/3}$, Cr $2p_{2/3}$ core-level spectra. In the Fe $2p_{2/3}$ spectrum, four corrosion product components were observed: Fe(II) oxide-Fe_{ox}^{2+}, Fe(III) oxide- Fe_{ox}^{3+}, Fe(III) hydroxide- Fe_{hyd} and LDH- Fe_x, with binding energies of 709.4, 710.7, 711.7 and 714.3 eV, respectively. In addition, as shown in the $Cr2p_{2/3}$ spectrum, Cr was present as Cr (III) oxide-Cr_{ox}^{3+}, Cr (III) hydroxide-Cr_{hyd} and Cr (VI) oxide-Cr_{ox}^{6+} at binding energies of 576.4, 577.4 and 578.8 eV, respectively. In addition, the exposure to UV illumination had no effect on the composition of the corrosion products of the 316 SS in salt lake atmosphere with respect to exposure time.

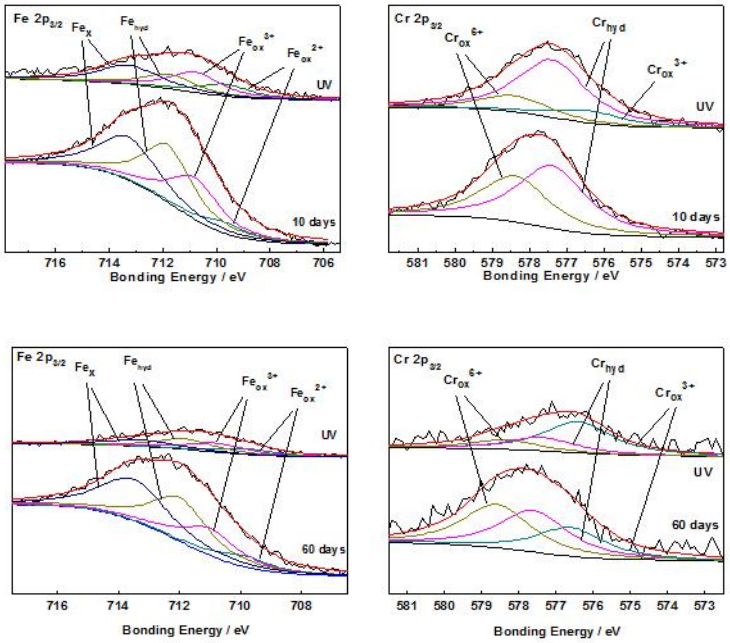

Figure 7. Effect of UV illumination on the corrosion product composition of 316 SS in salt lake atmosphere after 10 and 60 days.

The relative amount of [hydroxide] and [oxide] in the primary Cr and Fe compounds contained in the corrosion products are shown in Fig. 8. UV illumination had no significant effect on the type of corrosion products, however, had a significant effect on their relative amount. The relative amount of Fe_{hyd} under UV illumination was lower than that without UV illumination after 10 d, indicating that UV illumination inhibited the formation of Fe_{hyd}. However, the relative amounts of Fe_{ox}^{2+} and Fe_{ox}^{3+} after 10 and 60 d under UV illumination were slightly higher than those without UV illumination. In addition, UV illumination affected the relative amounts of Cr compounds. The relative amounts of Cr_{ox}^{3+} and Cr_{hyd} after 10 d under UV illumination were higher than those without UV illumination. In addition, the relative amount of Cr_{ox}^{3+} increased significantly after 60 d, whereas the relative amount of Cr_{hyd} under UV illumination was significantly lower than that without UV illumination. However, the relative amounts of Cr_{ox}^{6+} under UV illumination were lower than those without UV illumination. These results indicate that UV illumination promoted the formation of Cr_{ox}^{3+} and inhibited the formation of Cr_{hyd}. Previous studies have reported that Cr_2O_3 film is dense and usually exhibits superior protection, whereas $Cr(OH)_3$ film is loose, and exhibits weak protection [37,38]. Thus, the high Cr_2O_3 content in the passive film with an increase in corrosion time is favorable for improving the corrosion resistance of the 316 SS. Therefore, with an increase in the corrosion time, the corrosion rate of the 316 SS under UV illumination decreased (in Fig. 3d), which could be attributed to the increased protection of the corrosion products.

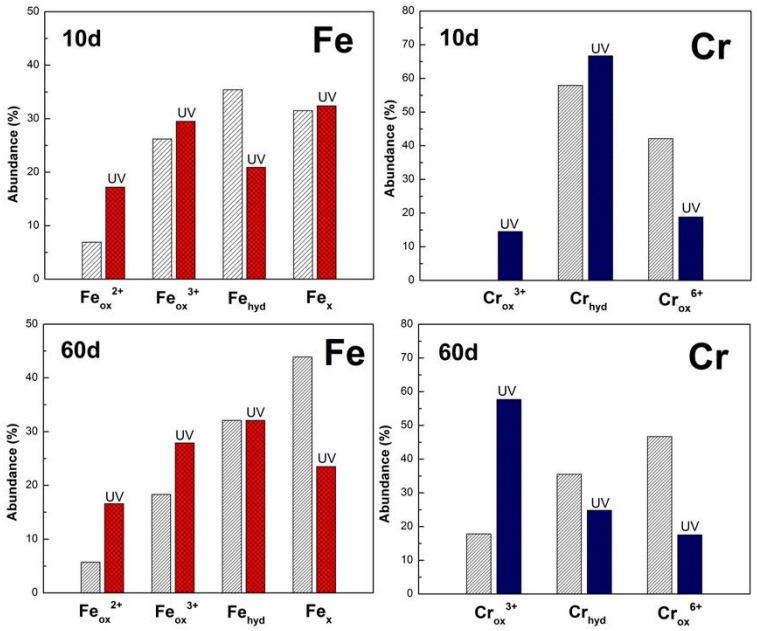

Figure 8. Effect of UV illumination on the relative amount of Fe/Cr-containing corrosion products after 10 and 60 days.

3.5. Corrosion mechanism

Fig. 9 shows the schematic illustratin of a model explaining the interaction mechnism between photons and semiconductor corrosion products such as n-type FeOOH and p-type Cr_2O_3, under UV illumination, which is similar to the model suggested by Gerischer and Burleigh [39,40]. The left part of the model represents the 316 stainless steel, the middle part represents FeOOH and Cr_2O_3, and the right side is the thin liquid film of $MgCl_2$. The lower part on the potential scale is positive, and the upper part is the negative potential.

FeOOH is a representative n-type semiconductor corrosion products, with conduction band (CB) and valence band (VB) potentials of 0.58 and 3.18 V (vs. SHE), respectively, The CB potential of FeOOH lies slightly above its Fermi level. Moreover, the redox potential of O_2/H_2O is 1.229 (vs. SHE), which is more positive than the Fermi level of FeOOH [8,41]. When FeOOH is covered with a thin liquid film of $MgCl_2$, the Fermi level of FeOOH moves toward a positive direction to reach an equilibrium value. Thus, the new Fermi level of FeOOH was located between the original Fermi level of FeOOH and the redox potential of O_2/H_2O. Consequently, the energy band of FeOOH at FeOOH / $MgCl_2$ solution interface shifts downward. In contrast, the Fermi level of the p-type semiconductor, Cr_2O_3, (CB-0.57 V, VB-2.93 V) lies slightly below its VB potential [42]. When Cr_2O_3 is covered with a thin liquid film of $MgCl_2$, the Fermi level of Cr_2O_3 will shift toward a negative direction to achieve an equilibrium value. Consequently, the energy band of Cr_2O_3 in the Cr_2O_3 / $MgCl_2$ solution interface shifts upward. The positions of the Fermi level, CB potential and VB potential of FeOOH and Cr_2O_3, formed on the 316 SS surface covered with a thin liquid film of $MgCl_2$ are also shown in Fig. 9.

The edge of the light absorption bands of FeOOH and Cr_2O_3 are 477 nm and 354nm, respectively. Consequently, under UV illumination, the corrosion products respond to the UV illumination to generate photogenerated electron-hole pairs. The corrosion mechanism of FeOOH and Cr_2O_3 on the 316 SS followed opposite trend. In addition, there may be a competition between the corrosion mechanism of FeOOH and Cr_2O_3. The electrons stored in the VB of FeOOH are excited into the CB, thus leaving holes in the VB, which leads to the separation of photogenerated electron-hole paris. Consequently, The electrons in the CB will flow down to the interface of $MgCl_2$ electrolyte, thus accelerating the oxygen reduction reactions. Meanwhile, the positive holes left in the VB flow into the 316 SS, and the holes capture the electrons generated during the anodic dissolution process of 316 SS and accelerated its atmospheric corrosion process. In contrast, the photogenerated electrons of Cr_2O_3 move to the surface of the 316 SS under UV illumination, thus providing cathodic protection for the 316 SS substrate. Consequently, the anodic dissolution of the 316 SS surface was prohibited. The corrosion tendency of the 316 SS under UV light illumination mainly depended on the relative content of Fe and Cr compounds. These results indicate that the relative amount of Cr_2O_3 increased gradually with an increase in the corrosion time, and the corrosion rate the 316 SS exposed to a simulated salt lake atmosphere was inhibited by UV illumination.

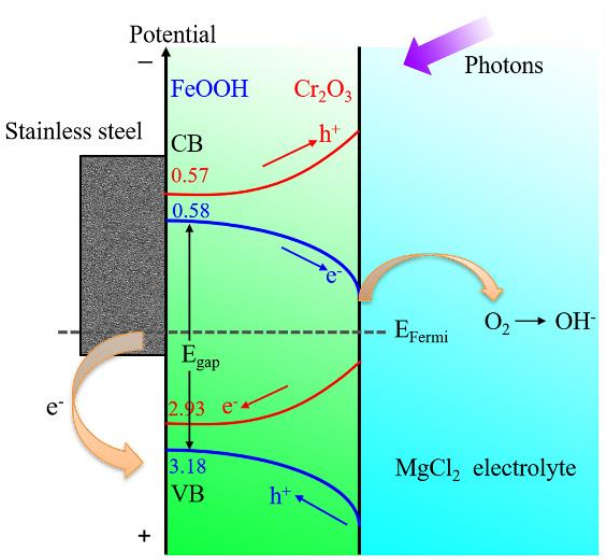

Figure 9. Schematic illustration of the interaction between photons and n-type FeOOH、p-tyte Cr_2O_3 semiconductors covered with $MgCl_2$ electrolyte under UV illumination.

5. CONCLUSION

In summary, the inhibitory effect of UV illumination on the atmospheric corrosion rate of 316 SS exposed to a simulated salt lake atmosphere was investigated. The corrosion rate was quantitatively characterized by the charge transfer resistance (R_{ct}), which was measured using in-situ EIS techniques.

The results revealed that UV illumination had no significant effect on the type of corrosion products but changed the relative amount of corrosion products, thus affecting the subsequent corrosion behavior of the 316 SS. In addition, UV illumination had a significant effect on the corrosion of the 316 SS in a salt lake atmosphere, which could be mainly attributed to the photovoltaic effect of the semiconducting corrosion products. Among them, the n-type semiconductor (such as FeOOH) and p-type semiconductor (such as Cr_2O_3) corrosion products had opposite effects on the corrosion process of the 316 SS under UV illumination.

ACKNOWLEDGEMENTS
The investigation is supported by National Natural Science Foundation of China (No. 51671197) and Liaoning Shenyang Soil and Atmosphere Corrosion of Material National Observation and Research Station.

References

1. C.G. Soares, Y. Garbatov, A. Zayed and G. Wang, *Corros. Sci.*, 51 (2009) 2014.
2. R. Lindstro, J.E Svensson and L.G Johansson, *J. Electrochem. Soc.,* 147 (2000) 1751.
3. C.L. Li, Y.T Ma, Y. Li and F.H Wang, *Corros. Sci.*, 52 (2010) 3677.
4. X.B. Liu and J.P. Liu, *Corros. Sci.,* 115 (2017) 129.
5. F. Mansfeld and J.V. Kenkel, *Corrosion,* 33 (2013) 13.
6. I.O. Wallinder and C. Leygraf, *Corrosion*, 73 (2017) 1060.
7. S. Sabir and A.A. Ibrahim, *Corros. Eng. Sci. Technol.,* 52 (2017) 276.
8. L.Y. Song, X.M. Ma, Z.Y. Chen and B.R. Hou, *Corros. Sci.,* 87 (2014) 427.
9. Y.W. Liu, J. Zhang, Y.H. Wei and Z.Y. Wang, *Mater. Chem. Phys.,* 237 (2019) 121855.
10. Z.Y. Chen, D. Liang, G. Ma, G.S. Frankel, H.C. Allen and R.G. Kelly, *Corros. Eng. Sci. Technol.,* 45 (2010) 169.
11. D. Liang, H.C. Allen, G.S. Frankel, Z.Y. Chen, R.G. Kelly, Y. Wu and B.E. Wyslouzil, *J. Electrochem. Soc*., 157 (2010) C146.
12. S. Fujimoto, T. Yamada and T. Shibata, *J. Electrochem. Soc.,* 145 (1998) 27.
13. D.D. Macdonald and D.F. Heaney, *Corros. Sci.,* 42 (2000) 1779.
14. M.X. Guo, Q. Yin, M.R Liu, C. Pan and Z.Y. Wang, *Acta Metall. Sin. (Engl. Lett.),* 33 (2020) 857.
15. T. Shinohara, S.I. Motoda and W. Oshikawa, *Mater. Sci. Forum.,* 475 (2005) 61.
16. X.M. Wang, X.G. Li and X.L. Tian, *Int. J. Electrochem. Sci.,* 10 (2015) 8361.
17. D.W. Zhang, F.C. Zhou, K. Xiao, T.Y. Cui, H.C. Qian and X.G. Li, *J. Mater. Eng. Perform.,* 24 (2015) 2688.
18. T. Akira and K. Toshiaki, *Corros. Sci.,* 42 (2000) 655.
19. A. Couet, A.T. Motta, A. Ambard and D. Livigni, *Corros. Sci.,* 119 (2017) 1.
20. C. Thee, L. Hao, J.H. Dong, X. Mu, X. Wei, X.F. Li and W. Ke, *Corros. Sci.,* 78 (2014) 130.
21. A.P. Yadav, A. Nishikata and T. Tsuru, *Corros. Sci.,* 46 (2004) 169.
22. X.N. Liao, F.H. Cao, L.Y. Zheng, W.J. Liu, A.N. Chen, J.Q. Zhang and C.N. Cao, *Corros. Sci.,* 53 (2011) 3289.
23. C. Pan, W.Y. Lv, Z.Y. Wang, W. Su, C. Wang and S.N. Liu, *J. Mater. Sci. Technol.,* 33 (2017) 83.
24. C. Pan, M.X. Guo, X. Lu, Z.Y. Wang and C. Wang, China Patent, 201910462067.X
25. L.M. Zhang, S.D. Zhang, A.L.Ma, H.X. Hu, Y.G. Zheng, B.J. Yang and J.Q. Wang, *Corros. Sci.,* DOI: 10.1016/j.corsci.2018.08.046.
26. K.W. Chung and K.B. Kim, *Corros. Sci.,* 42 (2000) 517.
27. Y.L. Cheng, Z. Zhang, F.H. Cao, J.F. Li, J.Q. Zhang, J.M.Wang and C.N. Cao, *Corros. Sci.,* 46

(2004) 1649.
28. S. Lenhart, M. Urquidi-Macdonald and D.D. Macdonald, *Electrochim. Acta,* 32 （1987） 1739.
29. P. Schmuki and H. Bohni, *Electrochim. Acta,* 40 (1995) 775
30. X.G. Feng, R.L. Shi, X.Y. Lu, Y.W. Xu, X.F. Huang and D. Chen, *Corros. Sci.,* 124 (2017) 150.
31. R.M. Fernandez-Domene, E. Blasco-Tamarit, D.M. Garcia-Garcia and J. Garcia Anton, *J Electrochem. Soc.,* 161 (2014) C25.
32. V. Vignal, C. Valot, R. Oltra, M. Verneau and L. Coudreuse, *Corros. Sci.,* 44 (2002) 1477.
33. Z.H. Dong, W. Shi, G.A. Zhang and X.P. Guo, *Electrochim. Acta,* 56 (2011) 5890.
34. M.X. Guo, Q. Yin, M.R. Liu, C. Pan and Z.Y. Wang, *Acta Metall. Sin. (Engl. Lett.),* 33 (2020) 101.
35. W. Han, G. Yu, Z. Wang and J. Wang, *Corros. Sci.,* 49 (2007) 2920.
36. M. Jonsson, D. Persson and D. Thierry, *Corros. Sci.,* 49 (2007) 1540.
37. T.Ishitsuka and K. Nose, *Corros. Sci.,* 44 (2002) 247.
38. J.P. Fu, Q.L Zhou, N. Li, Z.H. liu and T.S. Liu, *Corro. Sci.,* 104 (2016) 103.
39. H. Gerischer, *J. Electrochem. Soc.,* 113 (1966) 1174.
40. T.D. Burleigh, C. Ruhe and J. Forsyth, *Corrosion,* 59 (2003) 774.
41. Y. Xu and M.A.A. Schoonen, *Am. Mineral.,* 85 (2000) 543.
42. H. Tsuchiya, S. Fujimoto, O. Chihara and T. Shibata, *Electrochimi. Acta,* 47 (2003) 4357.